 FDMP, vol.7, no.1, pp.1-27, 2011

Onset of Hydrothermal Instability in Liquid Bridge. Experimental Benchmark

V. Shevtsova[1], A. Mialdun[1], H. Kawamura[2], I. Ueno[2]
K. Nishino[3] and M. Lappa [4]

Abstract: The experimental results from nine benchmark test cases conducted by five different groups are presented. The goal of this study is to build an experimental database for validation of numerical models in liquid bridge geometry. The need arises as comparison of numerical results with a single experiment can lead to a large discrepancy due to specific experimental conditions. Perfectly conducting rigid walls and, especially, idealized boundary conditions at the free surface employed in numerical studies are not always realized in experiments. The experimental benchmark has emphasized strong sensitivity of the threshold of instability to the liquid bridge shape. A clear distinction should be made between results belonging to the different disturbance patterns, i.e. different wave numbers. The results of benchmark contributors are in a satisfactory agreement when they are associated with the stability branch with an identical wave number. In this case the discrepancy of the results for determination of the critical parameters is about $\pm 15\% - 18\%$ and they can be used for the validation of numerical models.

Keywords: Marangoni, buoyancy, liquid bridge, experiment, instability.

1 Introduction

Thermocapillary convection refers to motions driven by spatial variation of surface tension σ in response to a temperature gradient along the interface. Flow will be driven for any surface-temperature gradients, no matter how small they are, see e.g. Schatz&Neitzel (2001). The present paper focuses on the study of thermocapillary convection in a half-zone or liquid bridge configuration, history of the problem one may find in the book by Lappa (2004).

[1] MRC, ULB, Belgium.
[2] Science University of Tokyo, Japan.
[3] Yokohama University, Japan.
[4] MARS, Napoli, Italy.
corresponding author is Shevtsova: vshev@ulb.ac.be

Liquid bridge consists of a fluid volume held by surface tension between two differentially heated horizontal flat co-axial disks; see sketch of the geometry in Fig. 1. A steady flow for small temperature differences consists of a single toroidal vortex and the motion at the interface is directed downward from the hot upper disk to the cold lower one. The strength of the thermocapillary convection is characterized by the Marangoni number Ma, the buoyant effect is characterized by the Rayleigh number, Ra and both depend on the Prandtl number, Pr :

$$Ma = \frac{\sigma_T \Delta T L}{\rho \nu \chi}, \quad Ra = \frac{\beta_T g \Delta T L^3}{\nu \chi}, \quad Pr = \frac{\nu}{\chi} \tag{1}$$

Here ρ is the density, ν is the kinematic viscosity, χ is the thermal diffusivity, β_T is the thermal expansion of liquid, $\sigma_T = -\partial\sigma/\partial T$, g is the gravitational acceleration, ΔT is the applied temperature difference and L is the length scale. Hereafter the height of liquid bridge d will be used as a length scale, $L = d$.

Many experiments have been performed in liquid bridges of high Pr fluids, such as silicone oils, because they are transparent, much less susceptible to free surface contamination than low Pr fluids, and their dependence upon temperature is well-defined. Although Prandtl number of molten silicon, $Pr = O(10^{-2})$, which has industrial interest, differs by two-three orders of magnitude for liquids used in liquid bridge experiments $Pr = O(10)$, it provides a lot of knowledge about thermocapillary convection and its instabilities.

A rich variety of phenomena associated with Marangoni convection was observed using silicone oils as a test liquid in ground and space experiments. A scaling law for the oscillation frequency at the threshold of instability, deduced from experiments with 5cSt silicone oil on the ground and under microgravity, was proposed by Carotenuto *et al.* (1997).

Ueno *et al.* (2003) studied oscillatory and chaotic thermocapillary convection using 1, 2 and 5 cSt silicone oils as test fluids. The same set of silicone oils was used by Tanaka *et al.* (2005) to study Particle Accumulation Structure (PAS).

In the experiments with silicone oils Kamotani *et al.* (2003), Shevtsova *et al.* (2005a) showed that the critical temperature difference is very sensitive to the heat loss at the interface.

In the microgravity experiments with 2cSt silicone oil Schwabe (2005) observed hydrothermal waves in a liquid bridge with aspect ratio near the Rayleigh limit.

Experimental evidence that the critical conditions for the onset of oscillatory flows in ground conditions strongly depends on the interface shape was suggested by Hu *et al.* (1994) who carried out experiments with 10 cSt silicone oil.

The measurements of dynamic free surface deformation due to thermal (Marangoni-

buoyant) convection was performed in liquid bridges of 5 cSt silicone oil using optical imaging by Shevtsova *et al.* (2008).

This list can be continued. However, a quantitative comparison of experimental and numerical results is a delicate question. The majority of numerical results, which are in good agreement are related to $Pr = 4$, see e.g. Leypoldt *et al.* (2000), Nienhüser and Kuhlmann (2002), Shevtsova *et al.*, (2003). Experimental results for this Pr are not demonstrative, because the corresponding fluid such as Acetone is volatile and the effect of evaporation is non-negligible.

Numerical simulations for high Pr liquids are very difficult due to the spike of isotherms near the cold wall. There exist a certain number of numerical publications related to high Pr number fluids by Lappa *et al.* (2001), Sim and Zebib (2002) Hu *et al.* (2003), Ermakov and Ermakova (2004), Shevtsova *et al.* (2009) etc. but direct comparison with experiment is rather seldom: see Irikira *et al.* (2004), Kousaka and Kawamura (2006).

As a rule, regardless geometry and specific boundary conditions, the critical Ma in numerical simulations with high Pr fluids is larger than the experimental one. Geometry, thermal boundary conditions and deformation of the interface in numerical models play an important role in determination of Ma_{cr} for any Pr number. In recent benchmark of the numerical solutions organized by Shevtsova, (2005) the results for the liquid bridge with $Pr = 0.01$ for the case of a straight interface were in an excellent agreement between participants, the scattering did not exceed 3%. However, for a deformed interface the scattering of the results has attained $\pm 15\%$. Obviously, high Pr fluids will make the situation worse. In these circumstances an experimental benchmark can be beneficial to provide some averaged values for the validation of advanced numerical models.

Five research groups took part in the Benchmark:
(a) [MRC], *ULB, Belgium* (Mialdun and Shevtsova);
(b),(c) two groups from *Tokyo University of Sciences (TUS)* :
(b)[TUS1] Kawamura, Takada;
(c) [TUS2] Ueno, Makino, Kawazoe and Enomoto;

Table 1: Physical properties of silicone oil

Silicone oil	ν (m^2/s)	κ (m^2/s)	ρ (kg/m^3)	β_T $(1/K)$	$\sigma_T = d\sigma/dT$ (N/mK)	σ (N/m)	Pr
5 cSt	$5 \cdot 10^{-6}$	$7.31 \cdot 10^{-8}$	912	$1.09 \cdot 10^{-3}$	$-6.37 \cdot 10^{-5}$	$1.97 \cdot 10^{-2}$	68

(d) [YU] *Yokohama University*, Japan (Tiwari, Nishino);
(e) [MARS] *MARS, Italy* (Dell′Aversana and Lappa).
Abbreviations of the institutions in square brackets will be used throughout the paper.

Note, that this experimental study has been performed on the "*no cost*" basis and, correspondingly, the participants have used the existing instruments. The target of the experimental benchmark is to determine the transition to oscillatory regime, i.e. the critical Ma number, the frequency near the threshold of instability and the structure of a hydrothermal wave.

2 Backgrounds

As a rule, experiments in liquid bridges are performed using heating from above to diminish the role of buoyancy. However, Velten *et al.* (1991) presented counterintuitive experimental results. For heating from below the critical Marangoni number for the onset of hydrothermal waves was nearly always larger than that obtained during heating from above. In agreement with these experimental findings, Wanschura *et al.* (1997) numerically showed for $Pr = 4$ that for heating from bottom, the onset of oscillatory convection is delayed to higher Marangoni numbers than for heating from above. Masud *et al.* (1997) also investigated the effect of heating orientation on Ma_{cr} and they found an opposite trend for liquid bridge of radius $R_0 = 3\,mm$, $Bd = 0.59$ and no effect for bridge of $R_0 = 1\,mm$, $Bo = 0.26$. Wanschura *et al.* (1997) also reported that additional buoyant force acts stabilizing on the axisymmetric flow for both heating and cooling from below, although the effect is small.

With the purpose to diminish the effect of buoyancy and for stability reasons the ground experiments are performed in small size systems. Accordingly, the typical height of the liquid bridge in laboratory experiments is about $(1-5)\cdot 10^{-3}m$. The dimensions of liquid bridges used by the participants are given in Table 2. The geometries are slightly different as the participants used the available set-up. The physical properties of 5 cSt silicone oil, $Pr = 68.4$, are listed in Table 1. It was suggested to use Dow Corning product, if possible.

An important factor for comparisons between experiments is the volume of the liquid contained in the bridge and, correspondingly, the interface deformation. Hereafter, the dimensionless volume is defined as $V \equiv \mathscr{V}/\mathscr{V}_0$, where $\mathscr{V}_0 = \pi R_0^2 d$ is the volume of the right–circular cylinder delimited by rods. Even in the situations when $V = 1$ the interface deformation caused by gravity depends on the size of LB and the physical properties of the liquid. The magnitude of the static deformation of the interface is determined by the ratio of the hydrostatic to the capillary pressure, i.e.

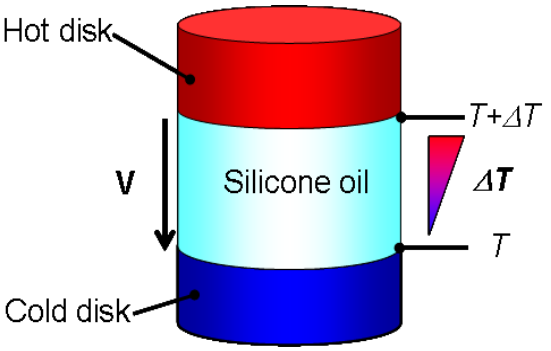

Figure 1: (online color) Sketch of liquid bridge.

by the so-called static Bond number.

$$Bo = \frac{\rho g d}{(\sigma_0/d)} = \frac{\rho g d^2}{\sigma_0} \tag{2}$$

The smaller is the Bond number, the less pronounced is the interface deformation by the gravity (e.g. when $V = 1$). The values of Bo are given in the last row of Table 2 for the case of unit aspect ratio, $\Gamma = d/R_0 = 1$.

In theoretical models interface deformation is rather often neglected, but experiments can not avoid it. Terrestrial (e.g. Hu *et al.* (1995), Masud *et al.* (1997)) and microgravity (Hirata *et al.* (1997)) experiments on high-Prandtl liquids (various silicone oils) revealed a non-monotonic behavior of the stability curve (ΔT_{cr}) versus the LB relative volume, see Fig. 2.

Knowledge of this stability diagram is a *key point* for the understanding the benchmark results. The diagram (ΔT_{cr} vs V) consists of two branches which formally can be assigned to small/ large volumes or slender/fat liquid bridges. For a liq-

Table 2: Geometry used; $\left(\times 10^{-3}[m]\right)$

Teams	MRC	TUS1	TUS2	YU	MARS
R_0	3	2.5	2.5	2.5	1.5
d	1.92	1.6	1.6		
	3.0	2.5	2.5	2.5	1.5
	3.6	3.0	3.0		
$Bo, d = R_0$	4.09	2.84	2.84	2.84	1.02

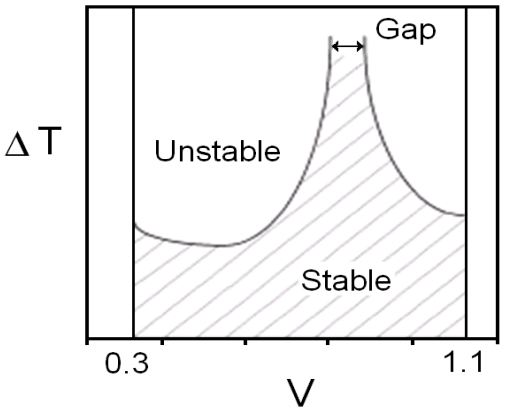

Figure 2: Experimental view of the stability diagramm for high Pr fluids.

uid volume roughly corresponding to a cylindrical interface the critical ΔT (or Ma number) has a peaked maximum indicating a very stable flow. In experiments this "peak" is transformed to a "gap", the width of which depends on how large values of ΔT can be achieved in the experiments.

Actually these branches on the stability diagram are two neutral curves with different wave numbers ($m = 1$ and $m = 2$ for $\Gamma \approx 1$) and they intersect at high ΔT_{cr}. The higher is Pr number, the sharper is the peaked maximum. However this intersection is difficult to reach experimentally and it was not the goal of the benchmark.

This diagram gives an idea why the numerically defined values of ΔT_{cr} (Ma_{cr}) are usually larger than experimental ones: calculations are performed for the cylindrical shape of liquid bridge, $V = 1$, while in the experiment the shape is a quasi-cylindrical and small deviations in the volume are possible due to non-ideality of the experiment.

The position of the peaked maximum depends not only on the volume, but on Bo and on the ambient conditions near the interface and, correspondingly, may be shifted to the left or to the right from one to another experiment.

3 Experimental

All the instruments employed in the benchmark have been used previously and more detailed description, than that below, can be found in corresponding references. The difference between the set-ups, shortly described below, is in the LB radius, the way of heating, the observation method and the surrounding conditions. Besides, the mean temperature in the set-ups of TUS1, TUS2 and YU was con-

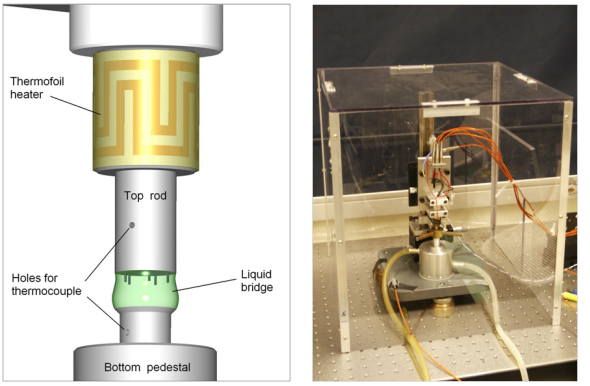

Figure 3: (online color) Sketch of liquid bridge and its photo in the laboratory used by MRC.

stant while for MRC and MARS it was changing (the temperature of the cold rod was constant). On one hand this dissimilarity can provoke justified criticism. On the other hand, diversity of set-ups is somewhat similar to the variety of numerical codes when some of them capture the certain phenomena better or worse.

The volume of liquid was measured with a good accuracy at all the experiments. For example, in the case of MRC syringe with a tolerance of 0.01 *mm* on a diameter of 2.30mm results in the error of 0.43%. The misfit of 0.07 *mm* on the total distance of 24mm between the expected length and the true traveling length leads to an additional error 0.29%. Thus, the overall volume error is 0.67%. TUS1, TUS2 and YU have used syringes of a similar class.

To prevent fluid from creeping over the edges of the rods, they have to be coated with an anti–wetting–barrier, which depends on the liquid and on the material of the rods. To omit anti-wetting coating and to reinforce arrangement, the lower rods in all benchmark set-ups are processed into a sharp edge to which menisci are attached.

The following methods have been used for detection of the onset of the oscillatory flow:

1) Thermocouples (TC) inside liquid: MRC, TUS1 and TUS2

2) Thermal sensor of the temperature oscillations on the surface: YU

3) Optical methods: (a) observation of an interference pattern of laser light from meridian plane (MARS); (b) oscillations of the interface (ULB); (c) particle motion (TUS1; TUS2)

The groups, who used thermocouples, have reported in the previous publications

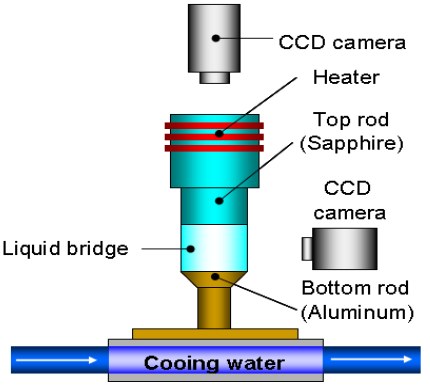

Figure 4: (online color) Sketch of liquid bridge setup used by TUS1 and TUS2

that their arrangement do not change the instability pattern.

The experimental apparatus used by the ULB team is similar to the one utilized in their past experiments, Shevtsova *et al.* (2005a), Mialdun&Shevtsova (2006). The general view of the set-up is shown in Fig. 3. To establish a fluid zone, a precisely defined amount of liquid was injected from a dedicated push syringe into the gap between the rods. The upper rod is constructed in such a way that three-dimensional displacements are possible. A heating Thermofoil^{TM} was mounted around the upper rod to heat the fluid from above. The lower rod was kept at a constant temperature using a thermo-regulated water-cooling system. Five shielded thermocouples ($D = 0.25mm$) were inserted inside the liquid at the same radial and axial positions and different azimuthal angles. These thermocouples were embedded into the liquid bridge through the upper rod to prevent disturbance of the free surface. The choice of 5 thermocouples enabled the determination of the critical wave number and the type of a hydrothermal wave without ambiguity. The temperature oscillations due to time-dependent convection were measured by thermocouples and by the oscillations of a free interface. The results were well agreed, see Ferrera *et al.* (2008). The displacement of the interface was measured optically using a previously developed technique (Montanero *et al.* (2008), Shevtsova *et al.* (2008)). The optical imaging allows the measurement of the free surface deviations from the corresponding equilibrium shape with an uncertainty of about 2 μm.

Two Japanese groups TUS1 and TUS2 have used similar set-ups shown in Fig. 4. The top rod is made of transparent sapphire, which enables to observe the flow field in the bridge through the rod. The bottom rod is made of sharp-tapered aluminum to sustain the contact line of the liquid bridge. The side surface of the bottom rod is coated with anti-wetting fluid. The upper rod was heated with an electrical

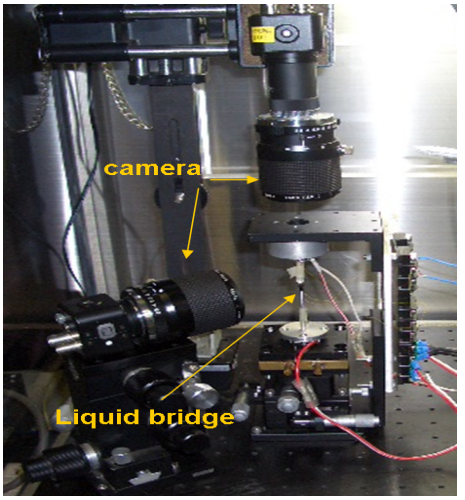

Figure 5: (online color) Photo of liquid bridge setup used by YU team

heater while the lower rod was cooled with cooling water; thus a constant mean temperature was maintained in the system. The temperature inside the liquid bridge was monitored by two $Cr-Al$ thermocouples ($D = 25\,\mu m$) inserted through the bottom rod. The thermocouples were located with 90° difference in the azimuthal direction. Silver-coated hollow glass spheres $D = 10\,\mu m$, $\rho = 1400 kg/m^3$ were added into the oil for flow visualization.

The onset of oscillations was monitored by observing particle motion through the top and by temperature oscillations on the thermocouples inside the liquid bridge ($100Hz$ sampling rate). More details about the experimental apparatus can be found in Ueno *et al.* (2003), Nishimura *et al.* (2005) The photo of the set-up, used by the YU team is shown in Fig. 5. As in the previous set-up the top rod is made of transparent sapphire and bottom rod is made of aluminum. One of the CCD cameras is mounted on the top of the sapphire rod and another one is placed in the horizontal plane at the level of liquid bridge. During the experiment the upper rod is heated while the bottom is cooled providing constant mean temperature in the system. A thermal sensor records the temperature signals on the surface of liquid bridge, see more details in Tiwari and Nishino (2010).

A sketch of set-up used by the MARS team is shown in Fig. 6. The temperature difference between the copper rods sustaining the liquid bridge was varied by heating the upper disk and keeping the temperature of the lower disk constant. Temperature was measured by thermocouples inserted into the copper rods as close as possible to the liquid bridge ends but without touching the oil to avoid disturbing the flow. The

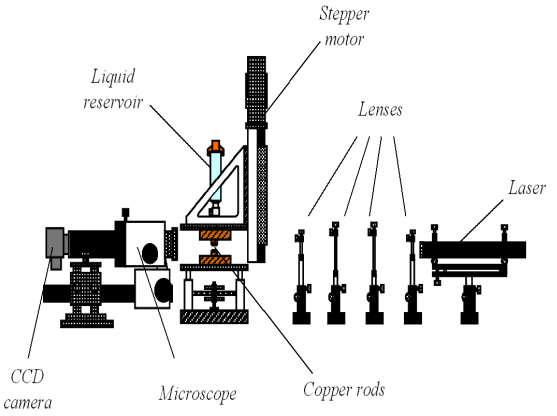

Figure 6: (online color) Sketch of liquid bridge setup used MARS team

onset of instability was detected through the observation of the interference pattern created by laser light used to illuminate a meridian plane of the zone itself. The laser beam was $< 0.2mm$ thick (1/e2 thickness), hence allowing direct detection of liquid-bridge surface oscillations induced by unsteady fluid motion. The liquid bridge was surrounded with a special optical glass cell to protect it from ambient air fluctuations. This cell had a square cross section to avoid undesired reflections and was used with thermal insulators at its open ends both to improve insulation from the outer air and to keep both copper rods un-coupled.

The bridge shape was varied by smoothly injecting or sucking liquid from the zone by an electro-pneumatic device. The bridge length was adjusted by 1-micron steps. It allowed automatic calculation the bridge volume with 10^{-2} cubic millimeter precision thanks to a video elaboration unit and to a dedicated software developed at MARS Center. The thermal expansion and evaporation of the oil were controlled during the measurements and they were compensated from time to time, by sucking or injecting required amount of liquid into the zone to keep V constant.

4 Liquid bridge shapes

Summarizing the experimental set-ups, three principally different types of the experimental set-ups have been used: (I) MRC with $R = 3\,mm$; (II) TUS1, TUS2 and YU with $R = 2.5mm$; (III) MARS with $R = 1.5\,mm$.

The free-surface shape of liquid bridge can be calculated by solving the Young-

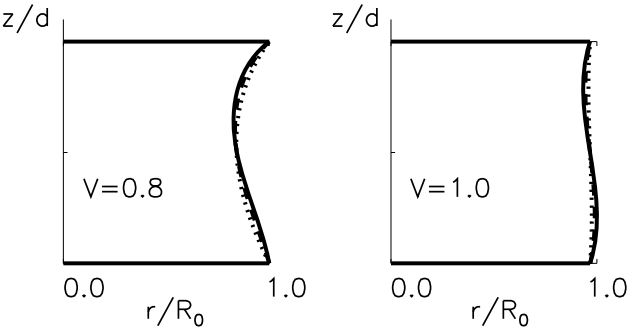

Figure 7: Dimensionalized liquid bridge shapes of benchmark participants when $\Gamma = 1$. Different lines correspond to various set-ups.

Laplace equation at prescribed static Bond number and aspect ratio.

$$\Delta P_{st} - Bo\, z = \frac{1}{N}\left[\frac{1}{h_0} - \frac{h_0''}{\Gamma^2 N^2}\right],$$
$$\text{where} \qquad N = \sqrt{(1+\Gamma^{-2}h_0'^2)} \tag{3}$$

Here $r = h_0(z)$ is the dimensionalized by radius position of the free surface and $h' = dh/dz$. The boundary conditions associated with this second order ordinary differential equation are:
1) Constant fluid volume (scaled by $\mathcal{V} = \pi R^2 d$) $V = \int_0^1 h_0^2(z)dz$.
2) fixed contact points $h_0(0) = h_0(1) = 1$
3) fixed contact angles: $\Gamma^{-1} h_z(0) = -cot\,\alpha_c$ or $\Gamma^{-1} h_z(1) = cot\,\alpha_h$.

Table 3: Contact angle α_h and apparent aspect ratio $\tilde{\Gamma}$ versus relative volume V

		$\Gamma = 1$		
		$V = 0.8$	$V = 0.9$	$V = 1.0$
MRC	α_h	34.79	52.56	69.81
	$\tilde{\Gamma}$	1.186	1.083	1.00
Japan	α_h	41.65	58.95	76.11
	$\tilde{\Gamma}$	1.188	1.084	1.00
MARS	α_h	51.28	67.98	85.04
	$\tilde{\Gamma}$	1.189	1.084	1.00

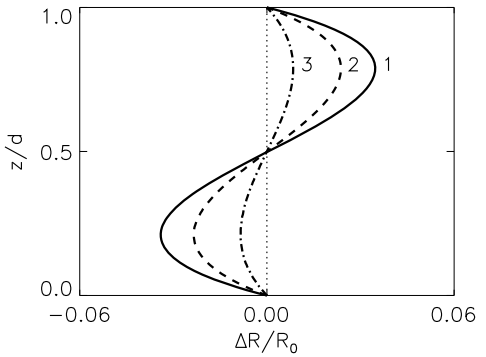

Figure 8: Magnified deviations of the interface shape from the straight when $V = 1, \Gamma = 1$; curves 1, 2, 3 correspond to MRC, Japan, MARS.

Here the angles α_c and α_h are measured from the cold and hot disks to the free surface. Thus three boundary conditions can be applied to solve the ordinary differential equation of the second order. Any two of these conditions may be used for the solution of eq. 3 and the third one determines ΔP_{st}, more details one may find in Shevtsova, (2005).

The calculated liquid bridge shapes for $\Gamma = 1$ and two volumes $V = 0.8, V = 1$ are shown in Fig. 7. The shapes from various set-ups for the same volume are not very different. Free surface deformation for unit volume, $V = 1$, looks small. The magnified shape deviations from the cylindrical one, shown in Fig. 8 for $V = 1$, clearly demonstrate that the larger is the Bond number, the stronger is the interface deformation: the upper part of LB becomes thinner and the bottom part bulges out.

Apparent aspect ratio can be introduced to characterize the shape effect, $\tilde{\Gamma} = d/h_0(z = d/2)$, where the radius of liquid bridge at mid-height is used instead of R_0. The detailed information about the benchmark shapes for $\Gamma = 1$ is summarized in Table 3, where α_h (angle near the hot rod) is given in addition to $\tilde{\Gamma}$. Note, that for $V = 1$ the both aspect ratios are equal, $\Gamma = \tilde{\Gamma} = d/R_0$, and with decrease of volume the apparent aspect ratio is increasing.

5 Results

Experimental study consists of 9 benchmark tests: to determine the critical parameters at the threshold of instability for three different volumes of liquid bridge ($V = 0.8, 0.9, 1.0$) and to examine three different aspect ratio for each of them, $\Gamma = 0.64, 1.0, 1.2$. Three groups (MRC, TUS1, TUS2) have carried out all the tests,

and two groups (YU, MARS) performed only three tests for $V = 1$. The outputs of each test are: the critical temperature difference, ΔT_{cr}, provided as a number of degrees in Kelvin with one digits after comma; the critical frequency, f_{cr}, provided in Hz with two digits after comma and the azimuthal wave number m at the threshold.

Hereafter a reader can find all the source data in Tables 5-11. The data for frequency are given in Hz while for ΔT_{cr} they are presented as the Marangoni numbers. The recalculation was done with the purpose to simplify the comparison of future simulations with benchmark results. For the prescribed aspect ratio Γ, the variable parameter in the experiments is the liquid bridge height, $d = \Gamma \cdot R$. Using the physical properties of 5cSt silicone oil from Table 1 will result in

$$Ma = 191.1\,\Delta T\,d, \qquad Bo = 0.454\,d^2 \tag{4}$$

To get final dimensionless values the height d should be put in mm and ΔT in Kelvin.

On physical side three independent physical quantities define the whole problem:

1) aspect ratio Γ,
2) dimensionless volume V,
3) applied temperature difference ΔT.

5.1 Stability diagram

When a certain temperature difference is exceeded (ΔT_{cr}), the thermoconvective flow undergoes transition from a steady axisymmetric to a three-dimensional oscillatory motion.

The effect of volume ratio on flow organization was discussed in Section 2. For all benchmark experiments the shape effect is important. The stability diagram built on the basis of the MARS results is shown in Fig. 9a for unit aspect ratio. It exhibits a rather large overstability gap, $0.7 < V < 0.9$. We should remind that the size of the gap is a conventional quantity and depends on maximal attainable ΔT in the experiment. Hereafter, we refer to a gap size at $Ma \approx 20\,000 - 30\,000$. Figure 9b combines points of all the other participants but for clarity the left branch of the MARS results is omitted. The solid lines connecting the points outline the belonging to the branch. To catch the location of the "overstability gap" one should look for two non-connected identical symbols. The results from Fig. 9b are summarized in Table 4. In the benchmark set-ups the margins of the overstability gap shifts to the side of a larger volume with the increase of the Bond number. Rough estimate of the mid-interval in Table 4 gives a hint that the peaked maximum of Ma_{cr} is shifted from $V \approx 0.8$ to $V \approx 0.95$ when the Bond number is changing from $Bo = 1.0$ to $Bo = 4.1$. The larger is the Bond number, the larger volumes are attached with the position of peak maximum.

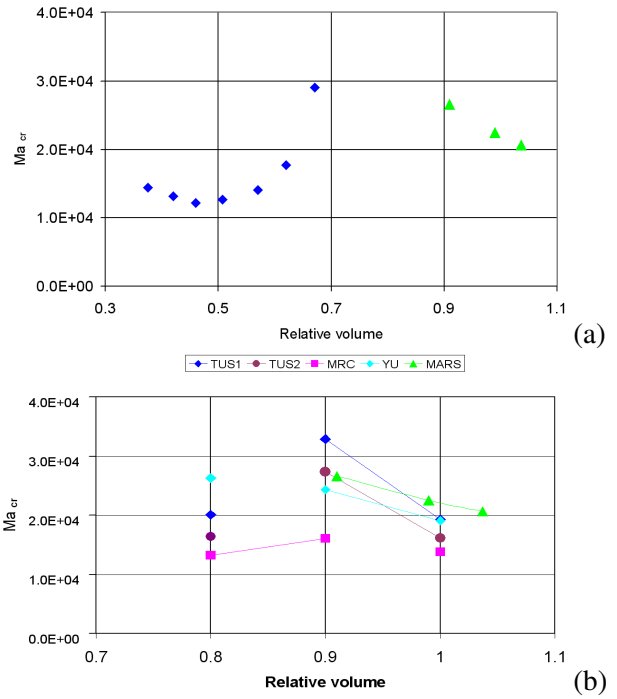

Figure 9: Stability diagram for LB with deformed interface, $\Gamma = 1$. (a) MARS results (b)All benchmark results for $V = 0.8, 0.9$ and 1.0.

Table 4: Provisional margins of the gap, $\Gamma = 1$.

Teams	MARS	TUS1, TUS2,YU	MRC
Bo	1.02	2.84	4.09
ΔV	$0.7 < V < 0.9$	$0.8 < V < 0.9$	$0.9 < V < 1.0$

The Bond and Prandtl numbers are not only the parameters which affect the position of the overstability gap. Non-obvious reason was recently found by Nishino, YU (private communication) who experimentally demonstrated that the position of the gap can be shifted to the side of small or large volumes by changing the surrounding conditions in the air near the interface.

5.2 Azimuthal wave number

For the considered fluid with high Prandtl number the flow pattern at the threshold of instability becomes periodic in space and in time. The hydrothermal wave above

the threshold of instability is characterized by integer azimuthal wave number m. As it was mentioned in Section 2 each branch on the stability diagram corresponds to a certain wave number. Preisser *et al.*, (1983) experimentally found the rule for determination of the critical wave number in a non-deformed liquid bridge

$$m_{cr} \cdot \Gamma \approx 2 \tag{5}$$

This dependence was numerically proved by Wanschura *et al.* (1995) and later re-confirmed in the experiments by Ueno *et al.* (2003). The present benchmark shows that this trend also holds in some cases for deformed bridges, e.g. for aspect ratio $\Gamma = 0.64$ the wave number is $m = 3$ regardless the examined volumes. For the aspect ratios $\Gamma = 1.0$ and 1.2 the wave number disperses between participants and shape effect should be taken into account. On the basis of numerical simulations for $Pr = 0.01$ in zero-gravity conditions Lappa *et al.* (2001) suggested

$$m_{cr}\tilde{\Gamma} = 2.$$

This behaviour is not confirmed here for high Pr liquids, the values of $\tilde{\Gamma}$ are given in Table 3 and the values of m in Table 5. On the other hand a relatively small range of volumes is examined to be used for validation of this ratio.

The benchmark results in Table 5 for $\Gamma = 1.2, V = 0.9$ shows that although TUS1 and TUS2 have used similar set-ups their wave numbers are not exactly the same. This can be only attributed to different mean temperatures and/or environmental conditions.

5.3 Critical Marangoni number

Sensitivity of critical parameters to the relative volume imposes additional difficulties on comparison between numerical and experimental results. The results are summarized in Tables 6-8 where the data for Ma_{cr} are given as five digits numbers. Ma_{cr} is re-calculated from ΔT_{cr} provided by the participants as values with

Table 5: Critical wave number versus relative volume V for different aspect ratio

	$\Gamma = 1$			$\Gamma = 1.2$		
V	0.8	0.9	1.0	0.8	0.9	1.0
MRC	1	1	2(?)	1	1	1
TUS1	1	2	2	1	?	1
TUS2	1	2	2	1	1	2
MARS		2	2			

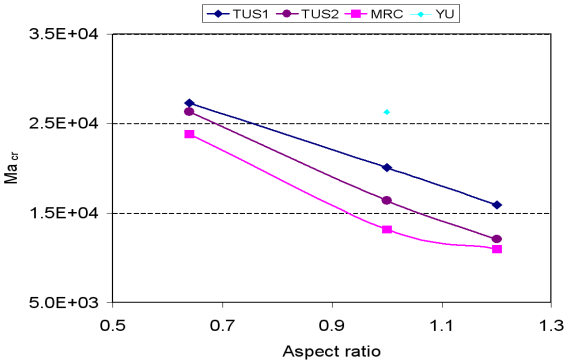

Figure 10: Critical Marangoni as function of aspect ratio, $V = 0.8$.

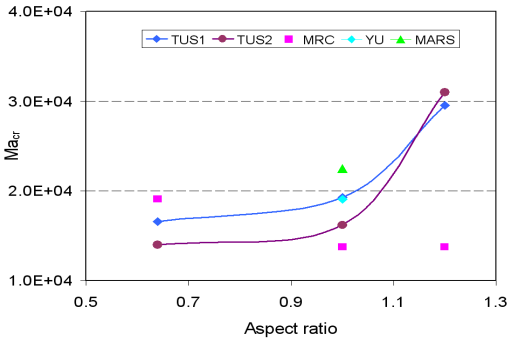

Figure 11: Critical Marangoni as function of aspect ratio, $V = 1.0$.

one digit after comma. The *benchmark values*, which are obtained by averaging the results for the identical wave number, are rounded. Figures 10-11 outline the tendency where the solid lines are drawn as a guide line.

The general trend is: when for a certain set of parameters the wave number in Table 5 is the same among the participants then the results for Ma_{cr} are consistent. For example, Fig. 10 shows a good agreement of the experimental results for $V = 0.8$. All the curves exhibit a similar tendency: the critical Marangoni number is diminishing with the increase of aspect ratio. The data of this plot are summarized in Table 6. The benchmark values are obtained by averaging the results of the three different values, and the dispersion of the results around the benchmark values does not exceed 7%.

The results agree poorly for $V = 0.9$, see Table 7. This volume corresponds to a region where neutral stability curves are close to the intersection and have a steep

Table 6: Ma_{cr} as a function of aspect ratio; $V = 0.8$

Teams	$\Gamma = 0.64$	$\Gamma = 1.0$	$\Gamma = 1.2$
TUS1	27 274	20 065	15 880
TUS2	26 326	16 387	12 097
MRC	23 849	13 186	11 007
YU		26 276	
benchmark value	26 000	19 000	13 000

Table 7: Ma_{cr} as a function of aspect ratio; $V = 0.9$

Teams	$\Gamma = 0.64$	$\Gamma = 1.0$	$\Gamma = 1.2$
TUS1	21 923	32 917	36 576
TUS2	17 459	27 327	26 372
MRC	20 180	16 052	12 383
YU		24 365	
MARS		26 625	
benchmark value	20 000	MRC n/a 28 000	n/a

Table 8: Ma_{cr} as a function of aspect ratio; $V = 1.0$

Teams	$\Gamma = 0.64$	$\Gamma = 1.0$	$\Gamma = 1.2$
TUS1	16 603	19 253	29 525
TUS2	14 004	16 196	30 958
MRC	19 079	13 759	13 759
YU		19 110	
MARS		22 500	
benchmark value	17 000	18 000	MRC n/a 30 000

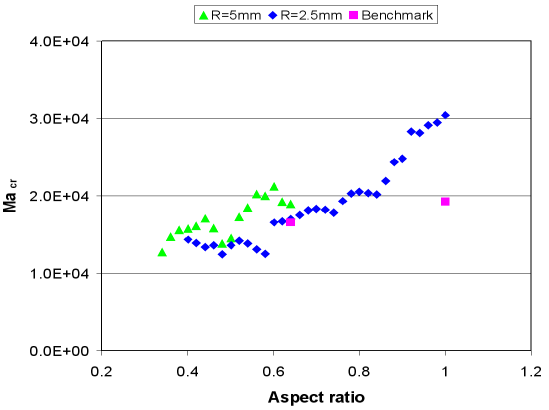

Figure 12: Critical Marangoni as function of aspect ratio, $V = 1.0$. Latest results of TUS1 with new apparatus. (courtesy Prof. H. Kawamura)

slope. Correspondingly, the values of the critical parameters are very sensitive to the small variations of the ambient conditions and the interface deformation. Results from different set-ups may fall either on a growing or on a lowering branches of the stability curve and it leads to a large scattering of Ma_{cr}. A good agreement is observed only for a small aspect ratio, $\Gamma = 0.64$, when all the results state $m = 3$: the dispersion of the results is about 10%. For $\Gamma = 1.0$ the dispersion of the results is larger, about 18% – excluding the MRC results, which are attached to another wave number.

The dependence of the critical Marangoni number upon the aspect ratio for volume ratio $V = 1$ is shown in Fig. 11 and summarized in Table 8. A unit volume ratio does not mean a straight cylinder although for the considered bridges the interface deformation is not very strong, see Fig. 8. For smaller $\Gamma = 0.64$ and, correspondingly, smaller Bo the dispersion of the results does not exceed 15%. For larger aspect ratio ($\Gamma = 1.2$) the MRC results differ from the other ones and this can be attributed to relatively large surface deformation, $Bo = 5.9$. It leads to a different wave number $m = 1$ and, correspondingly, to different values of the critical parameters.

The results from two identical set-ups TUS1 and TUS2 over the entire range of parameters display the scattering from 2% up to 10%. Major contribution to this divergence can be attributed to different surrounding conditions at which the experiments were performed.

Recently, the TUS1 group modified the set-up and performed a series of extensive experiments. They used a new apparatus where partition disks were employed: two horizontal plastic disks were placed perpendicular to the liquid bridge at the begin-

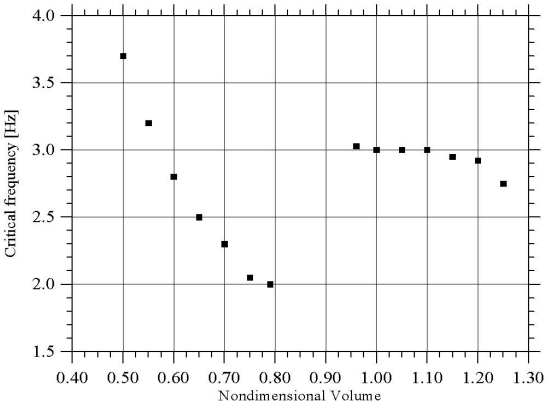

Figure 13: Critical frequency as function of volume ratio, $\Gamma = 1.0$. MARS results

ning of the solid rods to suppress/diminish the natural convection. The dependence of the critical Marangoni number on the aspect ratio is shown in Fig. 12 for two different radii of LB: 5*mm* (green triangles) and 2.5*mm* (blue rhombus). A wide range of aspect ratios was investigated in the new apparatus for a unit volume ratio, $V = 1$. The general tendency is that Ma_{cr} increases with the growth of aspect ratio. However, on a small scale regular jumps downwards are observed, which can be attributed to a change of the wave number. The two pink squares correspond to the benchmark results obtained by this team with the set–up presented in Fig. 4. The results are in a good agreement for $\Gamma = 0.64$ and rather different for $\Gamma = 1$. It seems that for a small LB height (i.e. $\Gamma = 0.64$) the influence of air motion is negligible, while for a relatively large height (i.e. $\Gamma = 1.0$) the suppression of the natural convection by partition disks raises the critical Marangoni number.

Table 9: f_{cr} as a function of aspect ratio; $\mathbf{V = 1.0}$.

Teams	$\Gamma = 0.64$	$\Gamma = 1.$	$\Gamma = 1.2$
MRC	$2.05\,Hz$	$0.67\,Hz$	$0.46\,Hz$
*TUS*1	$2.3\,Hz$	$1.27\,Hz$	1.52 Hz
*TUS*2	$2.06\,Hz$	$1.29\,Hz$	$1.58\,Hz$
MARS		$3.0\,Hz$	

5.4 Frequency at the threshold of instability

For silicone oils the onset of instability is the result of a supercritical Hopf bifurcation and the hydrothermal wave appearing at ΔT_{cr} is characterized by a critical frequency, f_{cr}. The critical frequency, f_{cr}, as well as Ma_{cr} is affected by the liquid bridge shape. By analogy with Ma_{cr}, the dependence f_{cr} versus V consists of two branches, attached to different wave numbers. The experimental results of the MARS team for $\Gamma = 1$, shown in Fig. 13, demonstrate this behavior. The frequency skip (jump) occurs when moving from one to another branch. The jump is observed rather often when the system changes the perturbation pattern. This jump of the frequency allows to determine more correctly the separation of branches on stability curve. Tables 9–11 summarize the measured frequency for different aspect ratios $\Gamma = d/R$ and relative volumes V. The oscillation frequency near the threshold depends on the liquid properties and the geometrical size of the liquid zone. Examining any arbitrary row in Tables 9–11 one can see that the frequency decreases with an increasing Γ for all set-ups (i.e. for all LB radii). The decrease of the frequency with the increase of LB height (i.e. aspect ratio) was earlier reported by Preisser *et al.*, (1983).

Table 10: f_{cr} as a function of aspect ratio; $\mathbf{V = 0.9}$

Teams	$\Gamma = 0.64$	$\Gamma = 1.$	$\Gamma = 1.2$
MRC	$2.1\,Hz$	$0.59\,Hz$	$0.42\,Hz$
*TUS*1	$2.5\,Hz$	$1.96\,Hz$	0.69 Hz
*TUS*2	$2.19\,Hz$	$1.78\,Hz$	$0.63\,Hz$

Table 11: f_{cr} as a function of aspect ratio; $\mathbf{V = 0.8}$

Teams	$\Gamma = 0.64$	$\Gamma = 1.$	$\Gamma = 1.2$
MRC	2.1 Hz	0.55 Hz	0.38 Hz
*TUS*1	2.98 Hz	0.68 Hz	0.56 Hz
*TUS*2	2.55 Hz	0.63 Hz	0.42 Hz
MARS		2.0 Hz	

Expectedly, all participants have reported that the variation of the frequency with volume and aspect ratio shows the same kind of behavior as Ma_{cr}. Thus the agree-

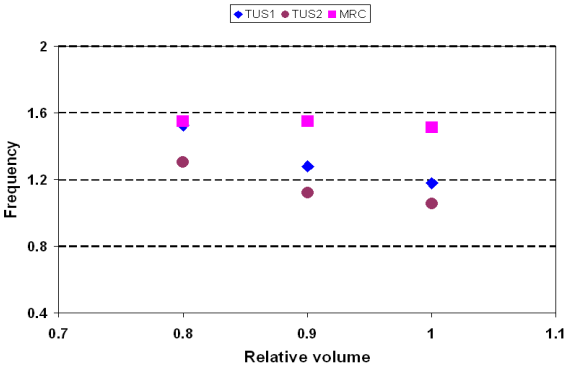

Figure 14: Critical frequency versus relative volume, $\Gamma = 0.64$. Frequency is scaled by viscous time, τ_{vis}, $[f] = f_{Hz}\,\tau_{vis}$

ment of the results for the frequency among participants also depends on the wave number m.

However, for the fixed Γ and V the value of frequency (in Hz) differs from one participant to another. For example, in Table 9 for $V = 1$ and $\Gamma = 1$ the critical frequency varies from $f = 0.67$ Hz up to 3 Hz. Choosing the proper dimensionless scale is a key point for comparing the results of different set-ups. Thermal convection includes two characteristic time scales - thermal, $\tau_{th} = d^2/k$, and viscous, $\tau_{vis} = d^2/\nu$. Their ratio determines the Prandtl number, $Pr = \tau_{th}/\tau_{vis} = \nu/k = 68$. It is very common to present the experimental results on frequency scaled by one of these times. In the case of normalization by thermal time the plot will be similar, just the values on the vertical axis will be multiplied by Pr.

Taking into account that for $\Gamma = 0.64$ all participants declare the same the wave number, their results should follow the same trend. Indeed, all results in Fig. 14 show diminishing f_{cr} with the increase of relative volume. In Fig. 15 the results for the measured frequencies are presented in another way. The frequency is shown as a function of the aspect ratio at $V = 0.8$. The results display quantitatively good agreement and are fixed to the same wave number $m = 1$. The frequency decreases with the increase of Γ for all set-ups (i.e. for all LB radii).

Analyzing the ground results for $NaNO_3$ in LB of different lengths, Preisser *et al.*, (1983) have suggested an alternative scaling for the frequency

$$F = f_{hz}\frac{d^2}{\chi\sqrt{Ma}}. \tag{6}$$

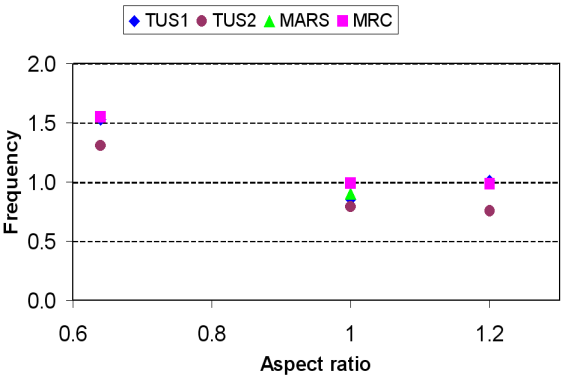

Figure 15: (online color) Critical frequency versus aspect ratio normalized by viscous time, $V = 0.8$

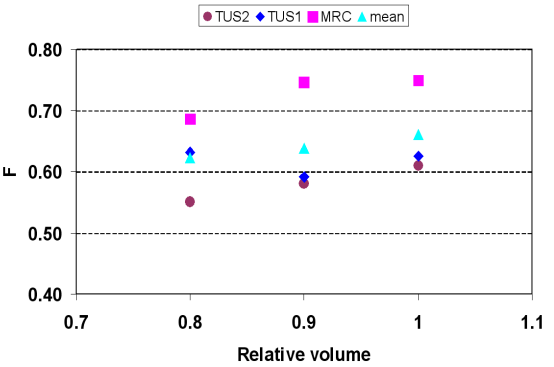

Figure 16: (online color) Dimensionless frequency $F = f_{hz}d^2/\chi\sqrt{Ma}$ versus relative volume, $\Gamma = 0.64$.

Benchmark results were checked against this formula. Formula (6) gives better fitting than viscous time for the dependence $f_{cr}(V)$ at fixed aspect ratio. Figure 16 and Fig. 14 present the same data using different normalizations. The dispersion of the results around the mean value in Fig. 14 is around 20%, whereas while using normalization by formula (6) it does not exceed 10%. However, for the dependence $f_{cr}(\Gamma)$ at fixed V, the scaling by viscous time provides a better fitting.

Another scaling law for frequency, deduced from experiments on the ground and under microgravity, was proposed by Carotenuto *et al.* (1997)

$$F_C = \frac{1}{2\pi}\frac{V_M}{\sqrt{(2Rd)}}Ma^{-1/3}. \tag{7}$$

where V_M is convective Marangoni velocity, $V_M = \sigma_T \Delta T / \rho \nu$. Taking into account Eqs.4 and Table 1 this scaling can be written only via variable quantities

$$F_C = 0.157 \cdot \sqrt{\Gamma}\, \Delta T^{2/3} d^{-4/3}\ [1/s], \tag{8}$$

where the height d should be put in *mm* and ΔT in Kelvin.

Benchmark results were also checked against formula (7). For liquid bridge with volume $V = 1$ it fits better than the scaling by the viscous time and by the formula (6). For volumes $V = 0.8$ and $V = 0.9$ the agreement is rather poor. Originally, the formula (7) was validated by the comparison with measurements in Space experiments.

6 Conclusions

This study presents the results of nine benchmark cases, which determine the critical parameters at the threshold of instability in liquid bridge configuration: the critical temperature difference, ΔT_{cr}, the critical frequency, f_{cr}, and the azimuthal wave number m. Measurements were carried out for high Prandtl liquid, $Pr = 68$, which is 5 cSt silicone oil. The considered LB relative volumes were $V = 0.8, 0.9,$ and 1.0, while the aspect ratios were chosen among those, which were often used in the previous experiments, i.e. $\Gamma = height/radius = 0.64, 1, 1.2$.

The benchmark was performed on "*no cost*" basis and, correspondingly, participants have used the existing instruments. Three different types of experimental set-ups were used: (1) MARS with $R = 1.5\,mm$; (2) TUS1, TUS2 and YU with $R = 2.5mm$; (3) MRC with $R = 3\,mm$. The difference between these set-ups was not only in the radius of LB but also in the way of heating, observation method, mean temperature, and surrounding conditions.

The experiments were performed in gravity conditions where the measured parameters have the strongest shape dependence. The stability diagramm (ΔT_{cr} vs V) consists of two neutral curves, rising ($m = 1$) and descending ($m = 2$), which intersect at the liquid volume that roughly corresponds to a straight cylinder. The closer to the intersection (peak maximum) the steeper is the curves behavior. Correspondingly, in this region of V the values of critical parameters are very sensitive to small variations of the ambient conditions, interface deformation and even skills of the experimentalist. Results from different set-ups may fall either on the rising or on the descending branch of the stability curve and it leads to the large scattering of ΔT_{cr} (Ma_{cr}).

On one hand the diversity of set-ups in the benchmark can be questioned. On the other hand it is somewhat similar to variety of numerical codes which are tackling the same problem. For example, numerical benchmark in deformed liquid bridges

for $Pr = 0.01$ (Shevtsova, (2005)) exposed scattering of the results about $\pm 15\%$. Although all contributors used the same body-fitted numerical method. The present experimental benchmark exposed similar level of scattering $\pm 15\% - 18\%$ when the results are associated to identical wave number.

Results from two identical set-ups TUS1 and TUS2 over the entire range of parameters display scattering in the range from 2% to 10%. This difference can be attributed to the various ambient conditions. Undoubtedly, the results of this benchmark will be useful for future numerical simulations.

A clear distinction should be made between region of volumes close to the peak area in the stability diagramm and those that are slightly away. For the latter case the results show a much smaller spread, hence the outcome from rather different set-ups are in better agreement with one another.

Keeping this in mind, we may state that the obtained *benchmark values* can be used for validation of numerical codes. Note that in the past the majority numerical results were obtained for the non-deformed free surface. The benchmark clearly demonstrated a necessity to develop numerical codes capturing interface deformation.

References

Carotenuto L., Castagnolo D., Albanese C. and Monti R., (1997): Instability of thermocapillary convection in a liquid bridge, *Phys. Fluids*, Vol. 10, pp. 555.

Chen Q.S., Hu W.R., and Prasad V. (1999): Effect of liquid bridge volume on the instability in small-Prandtl-number half zones, *J. Cryst. Growth*, Vol. 203, pp. 261.

Ermakov M.K., Ermakova M.S., (2004): Linear-stability analysis of thermocapillary convection in liquid bridges with highly deformed free surface, *J. Cryst. Growth*, Vol. 266, pp. 160-166.

Ferrera C., Montanero J.M , Mialdun A., Shevtsova V., Cabezas M. G., (2008): A new experimental technique for measuring the dynamical free surface deformation in liquid bridges due to thermal convection. *Meas. Sci. Technol.*, Vol. 19, pp. 015410.

Hirata A., Sakurai M., Ohishi N., Koyama M., Morita T., Kawasaki H., (1997): Transition process from laminar to oscillatory Marangoni convection in a liquid bridge under normal and microgravity", *J. Jpn. Soc. Microgravity Appl.*, Vol. 14, pp. 137-143.

Hu, W. R., Shu, J. Z., Zhou, R., Tang, Z. M. (1994): Influence of liquid bridge volume on the onset of oscillation in floating zone convection. *J. Cryst. Growth*, Vol. 142, pp. 379.

Hu W.R., Tang Z.M., Shu J.Z., Zhou R., (1995): Influence of liquid bridge volume on the critical Marangoni number in thermocapillary convection of half floating zone", *Microgravity Q.*, Vol. 5, No. 2, pp. 67-74.

Hu W.R., Tang Z.M., (2003): Influence of liquid bridge volume on the floating zone convection. *Cryst. Res. Technol.*, Vol. 38, pp. 627-634.

Irikira M., Arakawa Y., Ueno I., Kawamura H. ,(2005): Effect of ambient fluid flow upon onset of oscillatory thermocapillary convection in half-zone liquid bridge, *Microgravity Sci. Technol.*, Vol. XVI-I, pp. 174.

Y. Kamotani, L.Wang, L. Hatta, A.Wang, S. Yoda, (2003): Free surface heat loss effect on oscillatory thermocapillary flow in liquid bridges of high Prandtl number fluid, *Int. J. Heat and Mass Transfer*, Vol. 46, pp. 3211.

Kamotani Y., Matsumoto S. and Yoda S. (2007): Recent developments in oscillatory Marangoni convection. *FDMP: Fluid Dynamics & Materials Processing*, Vol. 2, pp. 147.

Kousaka Y. and Kawamura H. (2006): Numerical Study on the Effect of Heat Loss upon the Critical Marangoni Number in a Half-Zone Liquid Bridge, *Microgravity sci. technol*, Vol. XVIII-3/4

Lappa M., Savino R. and Monti R. (2001): Three dimensional numerical simulation of Marangoni instabilities in liquid bridges: influences of geometrical aspect ratio. *Int. J. Numer. Meth. Fluids*, Vol. 36, pp. 53-.

Lappa M., (2004): Fluids, Materials and Microgravity: numerical techniques and insights into Physics, Elsevier Science, 538pp. - ISBN 00-804-4508-X, Oxford, England.

Leypoldt J. , Kuhlmann H. C. and Rath H. J. (2000): Three-dimensional numerical simulations of thermocapillary flows in cylindrical liquid bridges, *J. Fluid Mech.*, Vol. 414, pp. 285.

Masud, J., Kamotani, Y., Ostrach, S. (1997): Oscillatory thermocapillary flow in cylindrical columns of high Prandtl number fluids. *AIAA J. Thermophys. Heat Transfer*, Vol. 11, pp. 105.

Mialdun A. and Shevtsova, V. M., (2006): Influence of interfacial heat exchange on the flow organization in liquid bridge. *Microgravity Sci. Technol.*, Vol. XVIII-3/4, pp. 146-.

Montanero J.M , Ferrera C., Shevtsova V., (2008): Experimental study of the free surface deformation due to thermal convection in liquid bridges. *Experiments in Fluids*, Vol. 45, pp.1087-1101.

Nienhüser Ch. and Kuhlmann H. C., (2002): Stability of thermocapillary flows in non-cylindrical liquid bridges, *J. Fluid Mech.*, Vol. 458, pp. 35-73.

Nishimura M., Ueno I., Nishino K. and Kawamura H. (2005): 3D PTV measurement of oscillatory thermocapillary convection in half-zone liquid bridge, *Exp. in Fluids*, Vol. 38, pp. 285-290.

Preisser F., Schwabe D. and Scharmann A. (1983): Steady and oscillatory thermocapillary convection in liquid columns with free cylindrical surface, *J. Fluid Mech.*, Vol. 17, pp. 112104-.

Schatz M.F. and Neitzel G. P., (2001): Experiments on thermocapillary instabilities. *Annu. Rev. Fluid Mech.*, Vol. 33, pp. 93-.

Schwabe D., (2005): Hydrothermal waves in a liquid bridge with aspect ratio near the Rayleigh limit under microgravity, *Phys. Fluids*, Vol. 17, pp. 112104-.

V. M. Shevtsova, D. E. Melnikov, J. C. Legros (2003): Multistability of oscillatory thermocapillary convection in a liquid bridge, *Phys. Review E*, Vol. 68, pp. 066311-.

Shevtsova V. (2005): Thermal convection in liquid bridges with curved free surfaces: benchmark of numerical solutions. *Journal of Crystal Growth*, Vol. 280, pp. 632-651.

Shevtsova V.M., Mialdun A., Mojahed M., (2005a): A study of heat transfer from liquid bridge interfaces to surroundings, *J. Non-Equilibrium Thermodynamics*, Vol. 30, pp.261-281.

Shevtsova V., Mialdun A., Ferrera C., Ermakov M., Cabezas M. G., Montanero J.M. (2008): Subcritical and oscillatory dynamic surface deformations in non-cylindrical liquid bridges, *FDMP: Fluid Dynamics & Materials Processing*, Vol. 4, pp. 43-.

Shevtsova V., Melnikov D.E., Nepomnyashchy A., (2009): New flow regimes generated by mode coupling in buoyant-thermocapillary convection, *Phys. Rev. Lett.*, Vol. 102, pp. 134503-.

Sim B-C., Zebib A., (2002) Effect of free surface heat loss and rotation on transition to oscillatory thermocapillary convection, *Phys. Fluids*, Vol. 14, pp. 225-231.

Tanaka S., Kawamura H. and Ueno I., (2006): Flow structure and dynamic particle accumulation in thermocapillary convection in a liquid bridge, *Phys. Fluids*, Vol. 18, pp. 067103-

Tiwari S. and Nishino K., (2010): Effect of confined and heated ambient air on onset of instability in liquid bridges of high Pr fluids, *FDMP: Fluid Dynamics & Materials Processing*, Vol.6, No.1, pp. 109-.

Tang Z.M. and Hu W.R. 1999, Influence of liquid bridge volume on the onset of oscillation in floating-zone convection III. Three-dimensional model, Adv. Space Res., Vol. 207 , pp. 239.

Velten R., Schwabe D., Scharmann A., (1991): The periodic instability of thermocapillary convection in cylindrical liquid bridges, *Phys. Fluids A*, Vol. 3, pp. 267-.

Ueno I., Tanaka S. and Kawamura H., (2003): Oscillatory and chaotic thermocapillary convection in a half-zone liquid bridge. *Phys. Fluids*, Vol. 15, pp. 408-.

Wanschura M., Kuhlmann H. C., and Rath H. J.(1997): Linear stability of two-dimensional combined buoyant-thermocapillary flow in cylindrical liquid bridges, *Phys. Rev. E*, Vol. 55.

Wanschura M., Shevtsova V. M., Kuhlmann H. C., and Rath H. J. (1995) Convective instability mechanisms in thermocapillary liquid bridges, *Phys. Fluids*, Vol. 5, pp. 912.